Camera Calibration from Images of Spheres

Hui Zhang, Kwan-Yee K. Wong, Guoqiang Zhang

Department of Computer Science, The University of Hong Kong, Pokfulam Rd, Hong Kong

{hzhang, kykwong, gqzhang}@cs.hku.hk

Abstract

This paper introduces a novel approach for solving the problem of camera calibration from spheres. By exploiting the relationship between the dual images of spheres and the dual image of the absolute conic (IAC), it is shown that the common pole and polar w.r.t. the conic images of 2 spheres are also the pole and polar w.r.t the IAC. This provides 2 constraints for estimating the IAC and hence allows a camera to be calibrated from an image of at least 3 spheres. Experimental results show the feasibility of the proposed approach.

Index Terms

Calibration, sphere, silhouette, surface of revolution (SOR).

I. INTRODUCTION

With the development of modern vision applications, multi-view vision systems have become more and more cost effective. The traditional way of calibrating such a large number of cameras requires the use of have some precisely made calibration patterns. However, such an approach is often tedious and cumbersome since points on the calibration pattern may not be simultaneously visible in all views. Besides, existing methods generally require knowledge of the metric structure [1][2] of the calibration pattern. This will involve the design and use of some highly accurate tailor-made calibration patterns, which are often difficult and expensive to be manufactured. To overcome these difficulties, it is desirable to have some common simple object, such as surfaces of revolution (SOR) [3] or spheres [4][5][6], to replace the calibration patterns.

This paper uses spheres as a calibration object. The silhouettes of a sphere can be extracted reliably from images, and this facilitates precise camera calibration. Besides, as long as the sphere is placed in the common field of view of the cameras, its occluding contours are always visible from any position and their images can be recovered even under partial occlusion. Spheres hence can be used to accurately calibrate multiple cameras mounted at arbitrary locations simultaneously. Spheres have first been used in [7] to compute the aspect ratio of the 2 image axes. Daucher et. al. [8] later introduced a multi-step nonlinear approach to estimate 4 camera parameters using spheres. However, error accumulated seriously in the separated steps. More recently, Teramoto and Xu [4] related the absolute conic with the images of spheres, and calibrated the camera by minimizing the reprojection errors nonlinearly. Nevertheless, the final results of their method depend greatly on the initialization. Agrawal and Davis [9] derived similar constraints as in [4] in the dual space. Their method first estimates the imaged sphere centers, and the remaining parameters are then solved by minimizing some algebraic errors with nonlinear semi-definite programming. However, there could be no solution when the noise is large. Further, apart from the 5 camera intrinsic parameters, 12 other parameters have to be estimated which might ruin the precision of the results.

This paper proposes an approach to solve the above problems by exploiting the relationship between the dual images of spheres and the dual image of the absolute conic. It is shown that a *conic homography* can be derived from the conic matrices of the imaged spheres, and the axis and vertex of such a homography are the pole and polar w.r.t. the image of the absolute conic. Some preliminary results have been published in [10]. Inspired by [3],

the polar thus obtained can also be regarded as the imaged revolution axis of a surface of revolution (SOR) formed by the 2 spheres. The pole then corresponds to the vanishing point of the normal direction of the plane formed by the camera center and the 2 sphere centers. This again gives the pole-polar relationship w.r.t. the IAC. The orthogonal constraints [11] can then be used to estimate the IAC from the pole and polar obtained, and calibrate the camera. Experiments show that this approach has a good precision and can be used directly in practical reconstruction.

This paper is organized as follows. Section II presents the theory for camera calibration from the imaged absolute conic. Section III relates the dual image of a sphere to that of the absolute conic (IAC). Section IV introduces our novel linear approach for camera calibration from spheres. Section V shows the results of synthetic and real experiments. Section VI discusses the degenerate cases, and Section VII gives the conclusions.

II. Calibration with the absolute conic

The absolute conic was first introduced by Faugeras et al. [12] for camera self-calibration. It is a point conic on the plane at infinity that is invariant to similarity transformation. Let the camera calibration matrix be

$$\mathbf{K} = \begin{bmatrix} \alpha f & s & u_0 \\ 0 & f & v_0 \\ 0 & 0 & 1 \end{bmatrix}, \tag{1}$$

where f is the focal length, α is the aspect ratio, (u_0, v_0) is the principal point and s is the skew. The image of the absolute conic (IAC) is then given by [12]

$$\omega = \mathbf{K^{-T}K^{-1}} = \begin{bmatrix} \omega_{11} & \omega_{12} & \omega_{13} \\ \omega_{12} & \omega_{22} & \omega_{23} \\ \omega_{13} & \omega_{23} & \omega_{33} \end{bmatrix}. \tag{2}$$

Note that ω is a symmetric matrix defined up to an unknown scale, hence it has 5 dof.

The image of the absolute conic, and its dual (DIAC) $\omega^* = \mathbf{K}\mathbf{K}^\mathbf{T}$ [11], are the 2D projections of the 3D invariant absolute conic (AC) and the dual of the absolute conic (DAC), respectively. The IAC and DIAC are imaginary point and line conics, from which the camera calibration matrix $\mathbf{K}$ can be easily obtained by Cholesky decomposition [13]. A camera with $s = 0$ so called a zero skew camera, and this results in $\omega_{12} = 0$. When both $s = 0$ and $\alpha = 1$, the camera is called a *natural camera*, and this results in $\omega_{12} = 0$ and $\omega_{11} = \omega_{22}$. The IAC ω can be estimated using the orthogonal constraints [11], which states that the vanishing point $\mathbf{v}$ of the normal direction of a plane and the vanishing line $\mathbf{l}$ of the plane must satisfy the pole-polar relationship w.r.t. ω, i.e.,

$$\mathbf{l} = \omega\mathbf{v}. \tag{3}$$

This provides 2 independent constraints on the elements of ω. Hence to fully calibrate a camera, at least 3 such conjugate pairs are needed; for a zero skew or a natural camera, at least 2 pairs are needed.

III. THE APPARENT CONTOUR OF A SPHERE AND ITS DUAL

This section relates the IAC with the image of spheres. Consider first a particular case where a camera $\mathbf{P}=\mathbf{K}[\mathbf{I}_3|\mathbf{0}]$ is viewing a sphere centered at the Z-axis (see Fig. 1(a)). The limb points $\mathbf{X}=[r\cos\theta\ r\sin\theta\ Z_0\ 1]^\mathbf{T}$ of the sphere always form a circle $\mathbf{C}_3$ with radius r on the plane $Z = Z_0$. The image points $\hat{\mathbf{x}}$ (see Fig. 1(b)) of $\mathbf{X}$ under $\mathbf{P}$ can be defined as

$$\hat{\mathbf{x}}=\mathbf{K}\,[\mathbf{I}_3|\mathbf{0}]\begin{bmatrix} r cos\theta \\ r sin\theta \\ Z_0 \\ 1 \end{bmatrix} = r\mathbf{K}\begin{bmatrix} 1 & 0 & 0 \\ 0 & 1 & 0 \\ 0 & 0 & Z_0/r \end{bmatrix}\begin{bmatrix} cos\theta \\ sin\theta \\ 1 \end{bmatrix}, \tag{4}$$

where $[r\,0\,Z_0\,1]$ is the generating point of the circle $\mathbf{C}_3$. Since the point $\mathbf{X}_u = [\cos\theta\ \sin\theta\,1]^\mathbf{T}$

lies on the unit circle $\mathbf{C}_u{=}diag\{1,1,-1\}$, the homography $\hat{\mathbf{H}}{=}\mathbf{K}diag\{1,1,\gamma\}$ transforms $\mathbf{C}_u$ to the image of $\mathbf{C}_3$ as $\hat{\mathbf{C}}{=}\hat{\mathbf{H}}^{-\mathbf{T}}\mathbf{C}_u\hat{\mathbf{H}}^{-1}$, where $\gamma = Z_0/r$.

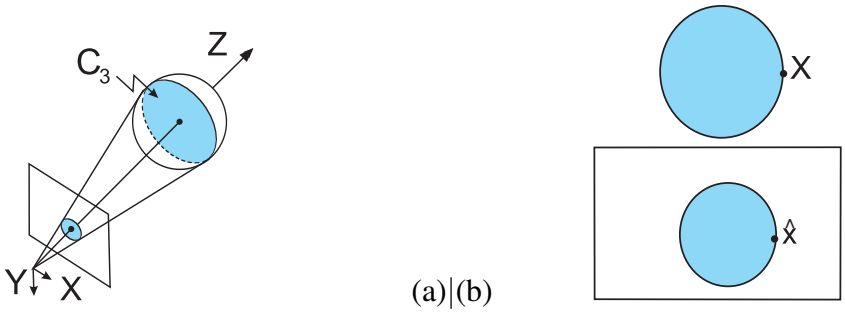

Fig. 1.(a) A sphere being viewed by a camera. (b) The limb points of the sphere is projected to a circle in the image.

Now consider the general case in which the sphere rotates about the camera center by a 3×3 rotation matrix $\mathbf{R}$. Let $\mathbf{H}{=}\mathbf{K}\mathbf{R}diag\{1,1,\gamma\}$, the image of the sphere is then given by $\mathbf{C} = \mathbf{H}^{-\mathbf{T}}\mathbf{C}_u\mathbf{H}^{-1}$. In the dual space, the dual of $\mathbf{C}$ is given by

$$\begin{aligned}\mathbf{C}^* &= \mathbf{K}\mathbf{R}diag\{1,1,-\gamma^2\}\mathbf{R}^{\mathbf{T}}\mathbf{K}^{\mathbf{T}} \\ &= \mathbf{K}\mathbf{R}(\mathbf{I}+diag\{0,0,-(\gamma^2+1)\})\mathbf{R}^{\mathbf{T}}\mathbf{K}^{\mathbf{T}} \\ &= \mathbf{K}\mathbf{K}^{\mathbf{T}} - (\gamma^2+1)\mathbf{K}\mathbf{r}_3\mathbf{r}_3^{\mathbf{T}}\mathbf{K}^{\mathbf{T}} \\ &= \mathbf{K}\mathbf{K}^{\mathbf{T}} - \mathbf{o}\mathbf{o}^{\mathbf{T}}, \end{aligned} \tag{5}$$

where $\mathbf{r}_3$ is the third column of the rotation matrix $\mathbf{R}$ and $\mathbf{o}{=}\sqrt{\gamma^2+1}\mathbf{K}\mathbf{r}_3$ is the image of the sphere center under $\mathbf{P}$. This result coincides with those derived in [9].

Note due to homogenous representation, a scalar β_i exists in the expression for each sphere image $\mathbf{C}_i$, i.e.,

$$\beta_i\mathbf{C}_i^* = \omega^* - \mathbf{o}_i\mathbf{o}_i^{\mathbf{T}}. \tag{6}$$

IV. CAMERA CALIBRATION

Based on the above derivation, this section introduces a linear approach to solve the problem of calibration.

A. CALIBRATION WITH ORTHOGONAL CONSTRAINTS

By eliminating the imaged sphere centers and the scalars, the orthogonal relationship in (3) can be directly obtained for calibrating the camera.

Proposition. *Given* $\mathbf{C}_1$ *and* $\mathbf{C}_2$ *which are* 3×3 *matrices representing 2 conic images, a homography* $\mathbf{H}_c = \mathbf{C}_2\mathbf{C}_1^*$*, termed as the conic homography, can be obtained. The eigenvectors of* $\mathbf{H}_c$ *give a fixed line (axis) and a fixed point (vertex) under the transformation introduced by* $\mathbf{H}_c$*, which are also the common pole and polar w.r.t.* $\mathbf{C}_1$ *and* $\mathbf{C}_2$*. Specifically, if* $\mathbf{C}_1$ *and* $\mathbf{C}_2$ *are the silhouettes of 2 spheres, the axis and vertex become the pole and polar w.r.t. the image of the absolute conic.*

Proof. It is straightforward to derive that the axis and vertex of $\mathbf{H}_c$, given by its eigenvectors, are the common pole and polar w.r.t. $\mathbf{C}_1$ and $\mathbf{C}_2$. Specifically, if $\mathbf{C}_1$ and $\mathbf{C}_2$ are the silhouettes of 2 spheres, multiplying the line $\mathbf{l} = \mathbf{o}_1 \times \mathbf{o}_2$ joining the images of the 2 sphere centers to both sides of (6) gives

$$\begin{aligned} \beta_1\mathbf{C}_1^*\mathbf{l} &= \omega^*\mathbf{l} \\ \beta_2\mathbf{C}_2^*\mathbf{l} &= \omega^*\mathbf{l}. \end{aligned} \tag{7}$$

Here $\mathbf{l}$ is also the vanishing line of the plane π passing through the camera center and the 2 sphere centers. It follows that

$$\begin{aligned} \beta_1\mathbf{C}_1^*\mathbf{l} - \beta_2\mathbf{C}_2^*\mathbf{l} &= \omega^*\mathbf{l} - \omega^*\mathbf{l} = \mathbf{0} \\ (\mathbf{C}_2\mathbf{C}_1^* - \frac{\beta_2}{\beta_1}\mathbf{I})\mathbf{l} &= \mathbf{0}. \end{aligned} \tag{8}$$

Hence $\mathbf{l}$ is an eigenvector of $\mathbf{H}_c$ corresponding to the eigenvalue β_2/β_1. $\mathbf{l}$ can be uniquely obtained from the eigenvectors of $\mathbf{H}_c$ since it is the only line having 2 intersection points

with both conics $\mathbf{C}_1$ and $\mathbf{C}_2$.

Let $\mathbf{v}$ be the vanishing point of the normal direction of π, so that $\mathbf{l}$ and $\mathbf{v}$ satisfy the orthogonal constraint (3). From (7),

$$\begin{aligned} \beta_1 \mathbf{C}_1^* \mathbf{l} &= \mathbf{v} \\ \beta_2 \mathbf{C}_2^* \mathbf{l} &= \mathbf{v}, \end{aligned} \tag{9}$$

hence

$$\begin{aligned} \frac{1}{\beta_1}\mathbf{C}_1\mathbf{v} - \frac{1}{\beta_2}\mathbf{C}_2\mathbf{v} &= \mathbf{l} - \mathbf{l} = \mathbf{0} \\ (\mathbf{C}_2^*\mathbf{C}_1 - \frac{\beta_1}{\beta_2}\mathbf{I})\mathbf{v} &= \mathbf{0}. \end{aligned} \tag{10}$$

This shows that $\mathbf{v}$ is an eigenvector of $\mathbf{H}_d = \mathbf{C}_2^*\mathbf{C}_1$ with corresponding eigenvalue β_1/β_2.

Let the eigenvectors of $\mathbf{H}_c$ be $\mathbf{l}_k$ with corresponding eigenvalues λ_k, i.e., $\mathbf{l}_k = \frac{1}{\lambda_k}\mathbf{C}_2\mathbf{C}_1^*\mathbf{l}_k$ ($k = 1, 2, 3$). The cross product of the 2 eigenvectors $\mathbf{l}_i$ and $\mathbf{l}_j$ ($i \neq j$) is given by

$$\begin{aligned} \mathbf{l}_i \times \mathbf{l}_j &= \frac{1}{\lambda_i}\mathbf{C}_2\mathbf{C}_1^*\mathbf{l}_i \times \frac{1}{\lambda_j}\mathbf{C}_2\mathbf{C}_1^*\mathbf{l}_j \\ &= \frac{\det(\mathbf{C}_2\mathbf{C}_1^*)}{\lambda_i\lambda_j}(\mathbf{C}_2\mathbf{C}_1^*)^{-\mathbf{T}}(\mathbf{l}_i \times \mathbf{l}_j) \\ &= \frac{\lambda_1\lambda_2\lambda_3}{\lambda_i\lambda_j}\mathbf{C}_2^*\mathbf{C}_1(\mathbf{l}_i \times \mathbf{l}_j). \end{aligned} \tag{11}$$

Without loss of generality, let $\mathbf{l}_1 = \mathbf{l}$, with corresponding eigenvalue $\lambda_1 = \beta_2/\beta_1$. The cross product of the other 2 eigenvectors $\mathbf{l}_2$ and $\mathbf{l}_3$ is therefore given by

$$\mathbf{l}_2 \times \mathbf{l}_3 = \lambda_1\mathbf{C}_2^*\mathbf{C}_1(\mathbf{l}_2 \times \mathbf{l}_3) \tag{12}$$

$$(\mathbf{C}_2^*\mathbf{C}_1 - \frac{\beta_1}{\beta_2}\mathbf{I})(\mathbf{l}_2 \times \mathbf{l}_3) = \mathbf{0}. \tag{13}$$

It follows that $\mathbf{v}$ is given by the cross product of the 2 remaining eigenvectors of $\mathbf{H}_c$. Hence, the axis $\mathbf{v}$ and vertex $\mathbf{l}$ of $\mathbf{H}_c$ are the pole and polar w.r.t. ω. Similarly, it can also be proven that $\mathbf{l}$ is the intersection of the 2 remaining eigenvectors of $\mathbf{H}_d$ and the vertex and axis of

$\mathbf{H}_d$ are the pole and polar w.r.t. ω.

Note that any 2 spheres can be regarded as a surface of revolution (SOR), with the revolution axis given by the line passing through the 2 sphere centers. It is easy to see that the vertex $\mathbf{l}$ and axis $\mathbf{v}$ of the conic homogaphy $\mathbf{H}_c$ correspond to the image of the revolution axis and the vanishing point of the normal direction of the plane π passing through the camera centers and the 2 sphere centers, respectively. This is exploited in [3] to derive the pole-polar constraints w.r.t. ω from the image of a SOR.

Given 2 sphere images, 2 linear constraints on the elements of the IAC can be obtained from the axis and vertex of the conic homography $\mathbf{H}_c$. Hence from 3 sphere images, 6 constraints can be obtained to fully calibrate a camera (see Fig. 2). When the number of

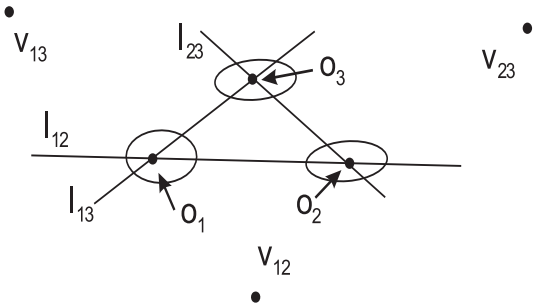

Fig. 2. Given 3 spheres, 3 conic homographies can be formed to give 3 pairs of axes and vertices. The camera can therefore be fully calibrated.

spheres reduces to 2, the camera with more than 2 unknown parameters cannot be calibrated. Additionally, increasing the number of spheres can increase the number of constraints and hence the precision of the calibration. Note that the number of constraints increases non-linearly with the number of spheres N, and is given by 2 times its combination of 2, i.e, $2 \times {}_N C_2$.

B. Multi-camera Calibration

By making use of the proposed algorithm, multiple cameras can be calibrated simultaneously by imaging 3 or more spheres at different locations. The internal parameters $\mathbf{K}_i$ of each camera are first obtained, and the imaged sphere centers $\hat{\mathbf{o}}_j^i$ (j being the index of the spheres) can be recovered as the intersections of the polars. The scalars κ_j^i ($\mathbf{o}_j^i = \kappa_j^i \hat{\mathbf{o}}_j^i$) can therefore be easily obtained from (6). Hence the 3D location of the sphere centers $\mathbf{O}_j$ w.r.t. the camera reference frame can be obtained as in [9], i.e.,

$$\mathbf{O}_j = \mathbf{K}^{-1}\mathbf{o}_j.$$

By registering the 2 sets of the 3D sphere centers, the camera relative rotation and translation parameters can be recovered analytically [14].

V. EXPERIMENTS AND RESULTS

A. Synthetic Data

The synthetic camera has focal length $f=880$, aspect ratio $\alpha=1.1$, skew $s=0.1$ and principle point $(u_0, v_0)=(320, 240)$. The points on the silhouette of each sphere were corrupted with a Gaussian noise of 16 different levels from 0 to 3 pixels, and the image of each sphere was obtained as a conic fitted to the noisy points [15].

Given 3 sphere images, the first experiment was to calibrate the camera under different noise levels. For each level, 100 independent trials were performed using our proposed approach, as well as Agrawal's semi-definite method. Fig. 3(a) shows the average percentage errors of the focal length. The errors of the other parameters, which are not shown here,

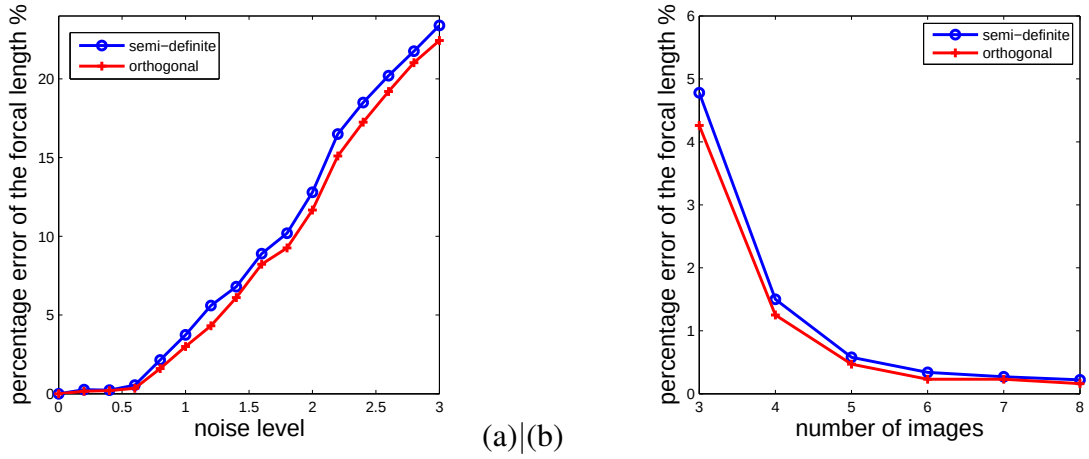

Fig. 3. (a) Relative errors of the focal length estimated under 16 different noise levels. (b) Relative errors of the focal length estimated from different number of imaged spheres under a noise level of 1 pixel.

exhibit similar trend. It can be seen that the errors increase linearly with the noise level. From Fig. 3(a), the approach with the orthogonal constraints has a slightly better precision than the semi-definite approach, which may be due to the less unknowns and calculation steps involved in the proposed approach. Table I shows the estimated parameters under the noise level of 1 pixel. The percentage errors [16] in the parameters w.r.t. the focal length αf are given in brackets.

In the second experiment, the camera was calibrated with different numbers of spheres, from 3 to 8, under a Gaussian noise of 1 pixel. For each number of spheres used, 100 independent trials were performed using the approach with orthogonal constraints, as well as Agrawal's semi-definite method. Fig.3(b) shows the average percentage errors of the focal length. Due to the fast increase in the number of constraints, it can be seen that the errors decrease exponentially as the number of spheres increases. Note that the approach with orthogonal constraints again performed slightly better than the semi-definite approach.

Approach	αf(% error)	f(% error)	s(% error)	u_0(% error)	v_0(% error)
Ground-truth	880	800	0.1	320	240
Semi-definite	838.16(4.75)	766.07(3.86)	2.38(0.26)	334.94(1.70)	238.52(0.17)
Orthogonal	839.24(4.63)	769.16(3.50)	1.28(0.13)	324.29(0.49)	242.97(0.34)

TABLE I
ESTIMATED CAMERA PARAMETERS FROM IMAGES OF 3 SPHERES UNDER A NOISE LEVEL OF 1 PIXEL.

B. Real Scene

In the real scene experiment, an image of 3 pingpong balls (see Fig.4(a)) was taken with a Nikon100D CCD camera. The image resolution was 1505×1000. The cubic B-spline snake [17] was applied to extract the apparent contours of the spheres, to which conics were fitted with a least square approach [15]. The camera was calibrated with the orthogonal approach and the results were compared with those from Agrawal's semi-definite approach. The estimated parameters are listed in Table II, where the result from the classical method of Zhang [2] is taken as the ground truth. Fig.4(b) shows the calibration pattern used with Zhang's calibration method. From Table II, it can be seen that the orthogonal approach has a better performance than the semi-definite approach.

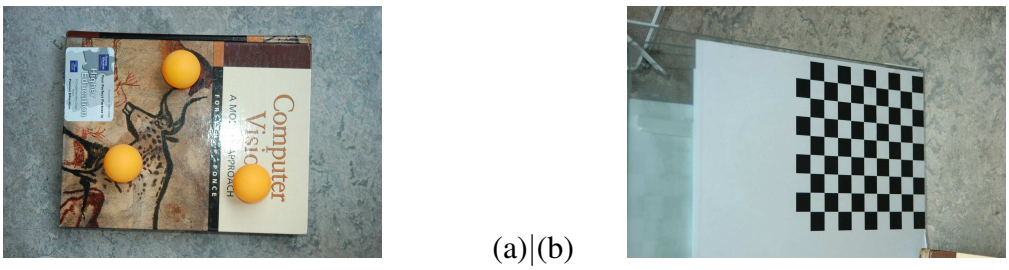

Fig. 4. (a) Image of 3 spheres. (b) Image of planar calibration pattern.

Approach	αf(% error)	f(% error)	s(% error)	(u_0(% error)	v_0(% error)
Zhang(ground truth)	3711.55	3692.00	0.10	776.47	438.45
Semi-definite	3515.33(5.29)	3523.27(4.55)	0.92(0.03)	777.94(0.04)	529.07(2.44)
Orthogonal	3641.35(1.89)	3651.84(1.08)	0.98(0.03)	772.26(0.11)	501.02(1.69)

TABLE II

CAMERA PARAMETERS ESTIMATED FROM THE PINGPONG BALL IMAGE WITH DIFFERENT APPROACHES.

C. Multi-camera calibration

In this experiment, 4 spheres were imaged by a network of 15 cameras. A 9×10 grid patten with $18mm \times 18mm$ squares was placed within the scene to provide background feature points for error analysis. The intrinsic parameters of each camera were first calibrated and the rotation and translation parameters of the other cameras with respect to the first one were recovered by registering the 3D sphere centers using the approach described in [14]. The fundamental matrix $\mathbf{F}_{ij}$ between an image pair was then recovered from the obtained camera intrinsic and extrinsic parameters. Note the intersection points of the pair of the inner bitangent lines to the sphere pairs provide 6 additional correspondences (see fig.5(a)). These points, together with the sphere centers, are mapped by $\mathbf{F}_{ij}$ to the other images. The second row of Table III lists the transfer errors for 3 arbitrary views selected from the camera network. The 72 inner corner points of the pattern in each image were extracted and mapped

Transfer errors (pixels)	View (1,2)	View(1,3)	View(2,3)
Centers & Intersections	0.59	0.87	0.39
Pattern(Orthogonal)	0.58	1.03	0.33
Pattern(Zhang)	0.45	0.67	0.53

TABLE III

RMS TRANSFER ERRORS (IN PIXEL) BETWEEN DIFFERENT IMAGE PAIRS IN A CAMERA TRIPLET.

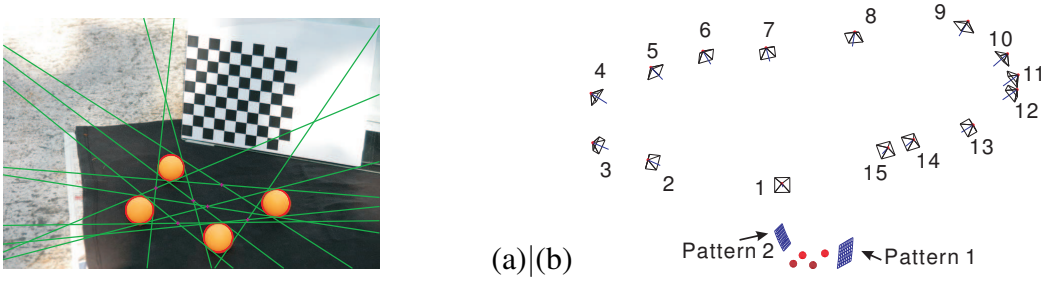

Fig. 5. (a) Image of the 4 spheres with a planar grid. The intersection points of the pair of the 2 inner bitangent lines the sphere pairs provide 6 correspondences. (b) The recovered grid patterns, spheres and the camera positions and orientations.

to the other image by the obtained $\mathbf{F}_{ij}$, and the transfer errors are listed in the third row of Table III. Note all the errors are about or less than 1 pixel. For comparison, the intrinsics of the stereo are also calibrated with Zhang's approach [2] and the transfer errors are listed in the last row of Table III. It can be seen that the errors are smaller than those from the orthogonal constraints. This is expected as these are exactly the errors being minimized in Zhang's approach.

Note the pattern, however, will be invisible to some cameras due to back-facing, e.g., in Fig. 5(b) pattern 1 is only visible to cameras 1 to 9. A second pattern was therefore put into the scene for testing the calibration results of the remaining cameras. In Fig. 5(b) pattern 2 is only visible to cameras 1 and 8 to 15. Given the recovered intrinsic and extrinsic parameters of the 15 cameras, the corner points of the 2 grid patterns were reconstructed, and the maximum distance from any reconstructed point to its corresponding grid point are only $3.0mm$ and $3.4mm$ for pattern 1 and pattern 2, respectively. Fig.5(b) shows the 2 reconstructed patterns, the 4 spheres and the camera positions and orientations.

VI. CRITICAL CONFIGURATION

When only 3 spheres are being used, there are a number of critical configurations in which the calibration process fails. First, when the polar of any 2 sphere images passes through or is close to the principle point, the calibration will not be accurate since the corresponding pole will be at infinity. Second, when the centers of the 3 spheres are collinear or the plane formed by the sphere centers passes through the camera center, only 2 constraints can be obtained and the camera cannot be calibrated. Third, when the line joining 2 sphere centers passes through the camera center, the sphere limb points become concentric so that less constraints will be obtained. However, all these degenerate cases can be easily avoided in practice to ensure a successful calibration, especially when more than 3 spheres are being used.

VII. CONCLUSIONS

This paper has proposed a simple algorithm to calibrate a camera network by making use of the apparent contours of at least 3 spheres in a single image. The solution can be used as a starting point for a maximum likelihood estimation which minimizes the reprojection error of the measured edgels. The performance of calibration could be poor if the spheres are imaged near the image centers or the borders. However, the key limitation of previous approaches, namely the low precision due to error accumulation in separate steps and the introduction of extra parameters, could be alleviated using the proposed approach.

REFERENCES

[1] Tsai R.Y., "A versatile camera calibration technique for high accuracy 3d machine vision metrology using off-the-shelf tv cameras and lenses," *IEEE Journal of Robotics and Automation*, vol. 3(4), pp. 323–344, 1987.

[2] Zhang Z., "A flexible new technique for camera calibration," *IEEE Trans. on Pattern Analysis and Machine Intelligence*, vol. 22(11), pp. 1330–1334, 2000.

[3] Wong K.-Y. K., Mendonça P. R. S., and Cipolla R., "Camera calibration from surfaces of revolution," *IEEE Trans. on Pattern Analysis and Machine Intelligence*, vol. 25(2), pp. 147–161, February 2003.

[4] Teramoto H. and Xu G., "Camera calibration by a single image of balls: From conics to the absolute conic," in *Proc. of 5th ACCV*, 2002, pp. 499–506.

[5] Ying X. and Hu Z., "Catadioptric camera calibration using geometric invariants," *IEEE Trans. on Pattern Analysis and Machine Intelligence*, vol. 26(10), pp. 1260–1271, Oct. 2004.

[6] Beardsley P., Murray D., and Zisserman A., "Camera calibration using multiple images," in *Proc. ECCV*, 1992, pp. 312–320.

[7] Penna M. A., "Camera calibration: A quick and easy way to determine the scale factor," *IEEE Trans. on Pattern Analysis and Machine Intelligence*, vol. 13, no. 12, pp. 1240–1245, 1991.

[8] Daucher D., Dhome M., and Lapreste J., "Camera calibration from spheres images," in *Proc. ECCV*, 1994, pp. 449–454.

[9] Agrawal M. and Davis L. S., "Camera calibration using spheres: A semi-definite programming approach," in *Proc. of IEEE International Conf. on Computer Vision*, 2003, pp. 782–789.

[10] H. Zhang, G. Zhang, and K.-Y. K. Wong, "Camera calibration with spheres: Linear approaches," in *Proc. International Conference on Image Processing*, Genova, September 2005, vol. II, pp. 1150–1153.

[11] Hartley R.I. and Zisserman A., *Multiple View Geometry in Computer Vision*, Cambridge University Press, UK, 2000.

[12] Faugeras O.D., Luong Q.-T., and Maybank S.J., "Camera self-calibration: Theory and experiments," in *Proc. ECCV*, 1992, pp. 321–334.

[13] Gentle J.E., *Numerical Linear Algebra for Applications in Statistics*, Springer-Verlag, 1998.

[14] Besl P. and McKay N., "A method for registration of 3d shapes," *IEEE Trans. on Pattern Analysis and Machine Intelligence*, vol. 14(2), pp. 239–256, 1992.

[15] Fitzgibbon A. W., Pilu M., and Fisher R. B., "Direct least-squares fitting of ellipses," *IEEE Trans. on Pattern Analysis and Machine Intelligence*, vol. 21(5), pp. 476–480, may 1999.

[16] Zhang Z., "Camera calibration with one-dimensional objects," *IEEE Trans. on Pattern Analysis and Machine Intelligence*, vol. 26, no. 7, pp. 892–899, July 2004.

[17] Cipolla R. and Blake A., "Surface shape from the deformation of apparent contours," *Int. Journal of Computer Vision*, vol. 9(2), pp. 83–112, November 1992.